A. Patterson,[a] N. C. Price[a] and J. Nairn[b]*

[a]Division of Molecular and Cellular Biology, Institute of Biomedical and Life Sciences, University of Glasgow, Glasgow G12 8QQ, Scotland, and [b]School of Biological and Environmental Sciences, University of Stirling, Stirling FK9 4LA, Scotland

Correspondence e-mail: jn2@stir.ac.uk

Unliganded structure of human bisphosphoglycerate mutase reveals side-chain movements induced by ligand binding

Erythrocyte-specific bisphosphoglycerate mutase is a trifunctional enzyme which modulates the levels of 2,3-bisphosphoglycerate (2,3-BPG) in red blood cells by virtue of its synthase and phosphatase activities. Low levels of erythrocyte 2,3-BPG increase the affinity of haemoglobin for oxygen, thus limiting the release of oxygen into tissues. 2,3-BPG levels in stored blood decline rapidly owing to the phosphatase activity of bisphosphoglycerate mutase, which is enhanced by a fall in pH. Here, the 1.94 Å resolution X-ray structure of bisphosphoglycerate mutase is presented, focusing on the dynamic nature of key ligand-binding residues and their interaction with the inhibitor citrate. Residues at the binding pocket are complete. In addition, the movement of key residues in the presence and absence of ligand is described and alternative conformations are explored. The conformation in which the ligand citrate would bind at the substrate-binding pocket is proposed, with discussion and representations of its orientation. The characterization of bisphosphoglycerate mutase–citrate interactions will provide a framework for the design of specific inhibitors of the phosphatase activity of this enzyme, which may limit the decline of 2,3-BPG in stored blood.

1. Introduction

2,3-Bisphosphoglycerate (2,3-BPG) modulates oxygen transport by binding preferentially to the deoxygenated haemoglobin tetramer, thus reducing oxygen affinity and facilitating the offloading of O_2 molecules in tissues where oxygen levels are depleted. Where 2,3-BPG concentrations are low, oxygen binds to haemoglobin with increased affinity and the dissociation of O_2 molecules in tissues is inhibited (Benesch & Benesch, 1969; Berger *et al.*, 1973). In normal human erythrocytes the concentrations of both 2,3-BPG and haemoglobin are ∼6 m*M* and they bind in a 1:1 molar ratio (Arnone, 1972).

The intracellular concentration of 2,3-BPG is maintained by the erythrocyte-specific enzyme bisphosphoglycerate mutase (BPGAM), a trifunctional enzyme that possesses mutase, synthase and phosphatase activities (Fothergill-Gilmore & Watson, 1989). A member of the larger acid phosphatase superfamily, which also includes fructose-2,6-bisphosphatase, pyrophosphatase and the 2,3-BPG-dependent phosphoglycerate mutase (PGAM), BPGAM shares striking sequence and structural similarity with the dimeric PGAM, suggesting a common ancestor (Fothergill-Gilmore & Watson, 1989). PGAM is ubiquitous in all tissues, predominantly catalysing the interconversion of 2- and 3-phosphoglycerate (mutase activity), with minimal synthase and phosphatase activities. In contrast, BPGAM is present exclusively in red blood cells and in comparison with PGAM displays an 800-fold lower mutase activity (Rose, 1982).

The normal erythrocyte concentration of 2,3-BPG can be altered under certain conditions, including anaemia, congenital heart disease and high altitude. These changes have been attributed to changes in blood pH and the availability of metabolites which affect the synthase and phosphatase activities of BPGAM (Mulquiney *et al.*, 1999; Mulquiney & Kuchel, 1999*a,b*). Of particular interest, however, is the observation that the levels of 2,3-BPG in stored blood are reduced. Indeed, it has been observed that current blood-storage systems maintain a normal erythrocyte 2,3-BPG concentration of ∼6 m*M* for

doi:10.1107/S1744309110035475   **1415**
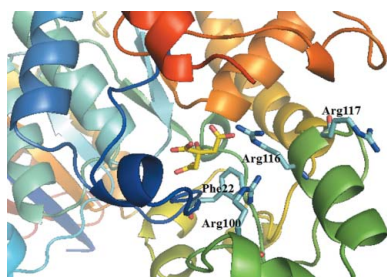
less than a week and all BPG is lost within 14 d (Raat *et al.*, 2005). The reduction in 2,3-BPG levels is accompanied by a decrease in erythrocyte levels of ATP, sialic acid and NO and an increase in 'bioreactive substances' such as histamine, lipids and cytokines. As a result, the shape of the erythrocyte changes, reducing the capacity of the cell to penetrate the capillaries and to offload its supply of oxygen where it is needed (Arslan *et al.*, 2005; Tinmouth & Chin-Yee, 2001). At alkaline pH it has been shown that BPGAM favours the synthase reaction; however, at lower pH the phosphatase reaction is dominant (Mulquiney *et al.*, 1999; Mulquiney & Kuchel, 1999*a,b*; Högman, 1998). Immediately after collection the pH of banked blood is 7.16, but it falls to 6.73 during storage owing to a build-up of lactic acid (Higgins & Klein, 1989). The change in pH is temperature-dependent and it is during the period between blood collection and storage that temperature appears to have a critical effect on pH and hence 2,3-BPG levels (Högman, 1998). The effects of temperature and pH are linked to the phosphatase activity of BPGAM. While storage solutions and buffers for the preservation of blood products have been described in the literature (Högman, 1998; Higgins & Klein, 1989; Högman *et al.*, 2002) and generally involve a citrate–dextrose solution and other metabolites such as adenine and phosphate, the problem of maintaining a balance between ATP and 2,3-BPG and of prolonging the viability of stored erythrocytes remains (Higgins & Klein, 1989; Ho *et al.*, 2003). Detailed knowledge of the structure of BPGAM including ligand-binding sites, catalytic residues and ligand-induced dynamics should allow the design, analysis and structural characterization of putative BPGAM phosphatase-specific inhibitors. Such small-molecule inhibitors could be used as additives in stored blood solutions, inhibiting the phosphatase activity of BPGAM without affecting other enzyme activities or the integrity of the erythrocyte and thereby potentially extending the shelf life of stored blood products.

A number of structures of homologous cofactor-dependent PGAMs isolated from a range of sources have been reported (Rigden *et al.*, 1999*a,b*; Crowhurst *et al.*, 1999; Bond *et al.*, 2001, 2002; Uhrinova *et al.*, 2001) as well some unrelated and structurally distinct cofactor-independent PGAMs (Jedrzejas *et al.*, 2000; Rigden *et al.*, 2003; Nukui *et al.*, 2007). The 2.5 Å resolution X-ray crystal structure of human BPGAM in the absence of ligands (Wang *et al.*, 2004) is incomplete, with some key side chains absent, including amongst others the binding-site residues Arg116 and Arg117. Our structure has all residue side chains intact from residue 2 (Ser) to residue 250 (Asp). In particular, residues Arg116 and Arg117 have been modelled, allowing a thorough inspection of the binding site and of potential side-chain movements in the presence and absence of ligand. In addition, a number of high-resolution structures of BPGAM complexed with substrates/effectors have been solved (Wang *et al.*, 2006). Comparison of these complexes with our 1.94 Å unliganded structure of BPGAM revealed a large (~3 Å) movement at the C^α backbone around Arg116/Arg117 and a distinctly large side-chain rearrangement of these residues. We have also modelled citrate into the active site of BPGAM and present isothermal titration calorimetry data, which clearly show the binding of citrate, a red blood cell metabolite and blood-storage additive (Högman, 1998; Higgins & Klein, 1989; Högman *et al.*, 2002).

2. Methods and materials

2.1. Plasmid construction

Standard protocols were used to ligate the gene encoding human bisphosphoglycerate mutase into vector pET30b (Novagen) for expression of protein with a C-terminal hexahistidine tag. Primers were designed with 5′-GGAATTC**CATATG**TCCAAGTACAAAC-3′ as the forward primer and 5′-CCG**CTCGAG**TTTTTTAGCTTG-TTTCACTTTTCC-3′ as the reverse primer to anneal to the gene encoding BPGAM, which was then amplified by PCR using *Pfx* polymerase (Invitrogen). The PCR product was blunt-cloned into pETBlue-1 and both strands were sequenced; the PCR product was then subcloned into pET30b at *Nde*I and *Xho*I (New England Biolabs) restriction sites. Correct insertion of the product was checked by performing restriction digests and sequencing of the coding region.

2.2. Protein expression and purification

Recombinant hexahistidine BPGAM was expressed in *Escherichia coli* BL21 (DE3) (Stratagene). Cell cultures were grown with shaking at 310 K in LB medium containing kanamycin at a concentration of 100 µg ml⁻¹. When the optical density at 600 nm reached 0.6, over-expression of BPGAM was induced by addition of IPTG to a concentration of 0.4 mM. Following a further 4 h of growth, cells were harvested by centrifugation. The cell pellet was resuspended in lysis buffer (buffer A; 50 mM Tris–HCl pH 8.0, 300 mM NaCl, 10 mM imidazole) and lysed by sonication on ice. Following centrifugation (50 000g for 60 min and 277 K), the supernatant was filtered and loaded onto a nickel-Sepharose column ($V_t \simeq 20$ ml; 1.6 × 10 cm; Pharmacia). Nonspecifically bound proteins were eluted with buffer A and BPGAM was subsequently eluted using a 200 ml imidazole gradient (from buffer A to buffer B, consisting of 50 mM Tris–HCl pH 8.0, 300 mM NaCl, 250 mM imidazole) with BPGAM eluting at 20% buffer B. BPGAM was judged to be >95% pure by SDS–PAGE. The concentration of protein was determined spectrophotometrically using an absorption coefficient value of 1.63 for a 1 mg ml⁻¹ solution at 280 nm, with a mass of 30 928 Da consistent with the amino-acid sequence of human BPGAM plus the hexahistidine tag. The mass of the purified protein was determined using electrospray mass spectrometry as described in Nairn *et al.* (1995).

2.3. Assay conditions

The mutase activity of BPGAM was determined at 298 K using an enolase-coupled assay, in which the formation of PEP was monitored at 240 mM. The 1 ml reaction vessel contained BPGAM at a concentration of 100 µg ml⁻¹, 30 mM Tris–HCl pH 7.0, 3 mM MgSO₄, 10 µM bisphosphoglycerate and 0.4 units of enolase and the reaction was started by the addition of 10 mM 3-PGA. The same assay was used for inhibition studies with varying concentrations of ligand and substrate. One enzyme unit is defined as producing an increase in absorbance of 0.1 min⁻¹.

2.4. Protein crystallization

Purified protein was buffer-exchanged into 20 mM Tris–HCl pH 7.5, 50 mM NaCl and concentrated to ~30 mg ml⁻¹. Crystals were grown by the hanging-drop method at 290 K as described by Wang *et al.* (2004), with the well solution consisting of 18–22% PEG 6K, 100 mM HEPES pH 6.8–7.2. Crystals, which generally grew within one week, were mounted on loops and flash-frozen in liquid nitrogen prior to data collection.

2.5. Data collection, processing and structure refinement

180 images were taken, each at 1° rotation, on BM14 at ESRF Grenoble. Data were indexed, integrated, scaled and refined using *MOSFLM*, *SCALA* and *REFMAC*5 from *CCP*4 (Collaborative

Table 1
Data-collection and refinement statistics for BPGAM.

Values in parentheses are for the highest resolution shell.

Data collection	
X-ray source	ESRF Grenoble BM14
Space group	$P12_11$
Unit-cell parameters (Å, °)	$a = 38.5$, $b = 61.3$, $c = 122.7$, $\alpha = 90$, $\beta = 95.8$, $\gamma = 90$
Resolution range (Å)	122.17–1.94 (2.04–1.94)
No. of reflections	40076
Reflections used	38075
Completeness	95.0 (84.9)
$\langle I/\sigma(I)\rangle$	6.7 (2.0)
R_{merge}	0.062 (0.281)
Multiplicity	3.6 (3.4)
Refinement	
No. of atoms	5089
No. of water molecules	1015
R factor	0.176
R_{free}	0.244
B factor (Wilson plot) (Å^2)	25.49
PDB code	3nfy

Table 2
Distances (in Å) from backbone N atoms of BPGAM (PDB entry 3nfy) to citrate compared with PGAM–citrate (1yfk) and BPGAM–2,3-BPG (2hhj).

	BPGAM–citrate model	PGAM–citrate (chain A/chain B)	BPGAM–BPG
Cys(Ser)23 N—O4	2.79	2.57/3.68	2.79 (BPG O8)
Ser(Gly)24 N—O4	3.23	3.07/2.93	3.30 (BPG O8)
Ser(Gly)24 N—O3	3.09	3.12/3.31	3.24 (BPG O7)
Tyr92 N—O3	7.07	6.09/5.67	6.05 (BPG O7)
Phe22 N—O5	6.26	8.09/5.07	6.46 (BPG O5)
Arg116 N—O1	7.84	6.57/6.71	8.10 (BPG O5)
Arg117 N—O1	7.91	7.05/6.75	8.51 (BPG O5)
Arg117 N—O2	10.04	7.67/8.57	

Computational Project, Number 4, 1994). *SHELX*97 was used to refine side-chain occupancies (Sheldrick, 2008). The published 2.5 Å resolution structure of BPGAM (PDB code 1t8p; Wang *et al.*, 2004) was used as a model. Manual refinement of the structure was performed using *Coot* (Emsley & Cowtan, 2004).

2.6. Modelling citrate into BPGAM

Using the available complex structures of PGAM bound with citrate (PDB code 1yfk; Wang *et al.*, 2005) and of BPGAM bound with BPG (PDB code 2hhj; Wang *et al.*, 2006) as guides, citrate was modelled into the binding site of BPGAM (PDB code 3nfy). *Coot* (Emsley & Cowtan, 2004) was used to superimpose the PGAM–citrate complex onto the BPGAM structure, giving a good approximation of the conformation of citrate at the binding site, which was then refined by hand. This model was further refined using the ligand-docking program *DOCK* (Kuntz *et al.*, 1982) by inputting the BPGAM–BPG complex structure (PDB code 2hhj) to identify the binding site and subsequently using citrate as the potential ligand.
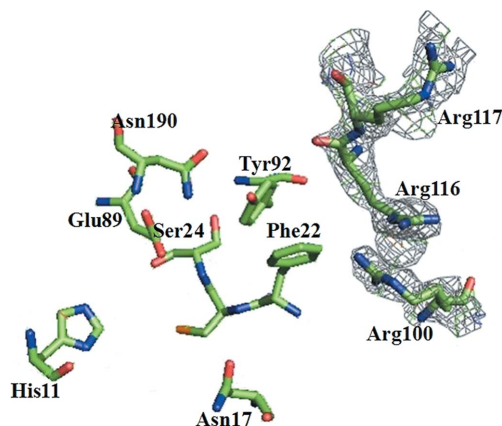
Figure 1
The binding pocket of BPGAM (PDB entry 3nfy), showing amino acids Arg116, Arg117 and Arg100 in electron density. The orientations of the side chains of these residues differ from the orientations of the side chains of Arg116, Arg117 and Arg100 in the BPGAM–BPG complex structure (PDB entry 2hhj), suggesting a large degree of movement upon ligand binding.

2.7. Isothermal titration calorimetry

Citrate binding to BPGAM was measured using isothermal titration calorimetry (ITC) based on the method described by Nairn *et al.* (2000). In these experiments, the protein concentration was typically 1.84 mg ml^{-1} (30 µ*M*) and the citrate concentration used for injection was 1.182 m*M*. After 60 s, 1 µl ligand solution was injected into the reaction cell, followed by a further 28 × 10 µl injections at 180 s intervals. An average apparent association factor was calculated from five independent ITC measurements.

3. Results

Crystallization of human BPGAM resulted in the formation of two crystal forms. One of these had a rod-shaped morphology and did not diffract. The other was a more regular cubic form that gave good diffraction. Data were collected to 1.94 Å resolution. The crystallographic statistics are given in Table 1.

Main chains *A* and *B* have been modelled into density from residue 2 (serine) to residue 250 (aspartic acid). In addition, the side chains of certain key residues, which had been absent from chains *A* and *B* in the previously available uncomplexed structure (Wang *et al.*, 2004), have been added. These include Arg116 and Arg117, which lie at the entrance to the active site (Fig. 1).

The side chains of the surface residues Lys5 (chain *A*), Glu110 (chains *A* and *B*), Gln134 (chain *A*) and Asp237 (chain *B*), which were absent from the structure of Wang *et al.* (2004), have also been added.

Citrate was modelled into the entrance of the BPGAM active site (Fig. 2). Comparison of this model with our unliganded structure revealed a number of structural differences around proposed ligand-binding residues, namely Arg100, Arg116 and Arg117 (Nairn *et al.*, 2000). Positioning citrate at the entrance to the binding site of BPGAM resulted in significant movement of the side chains of Arg100, Arg116 and Arg117. The distances between citrate and the binding-site residues of BPGAM are summarized in Table 2. These distances compare favourably with comparable interactions in the PGAM–citrate complex (1yfk) and the BPGAM–BPG complex (2hhj).

Measurements of ligand occupancy at the binding site of X-ray crystal complex structures have been well described in the literature (Wu *et al.*, 2001; McNae *et al.*, 2005). This technique has been used here to measure the occupancy of the critical ligand-binding arginine residues. An occupancy refinement of the side chain of Arg116 gives an occupancy of 69% position 1 (directed away from the binding site, with a distance of 8.23 Å between NH2 and C1 of citrate) and 31% position 2 (directed in towards the binding site, with distances of 3.4 Å between NH2 and the O2 atom of citrate and of 2.67 Å between NE and C1). In comparison, the distances between Arg116 and

citrate in the complex with PGAM (1yfk) are 3.79 Å for NH2–Cit O1 and 2.84 Å for NE–Cit O1. In the BPGAM–BPG structure (2hhj), the distances between Arg116 NH2 and the three O atoms of the 2-phosphate group of 2,3-BPG are 3.13 Å (O13), 3.48 Å (O14) and 4.95 Å (O15). Similar distances were observed when 2,3-BPG was
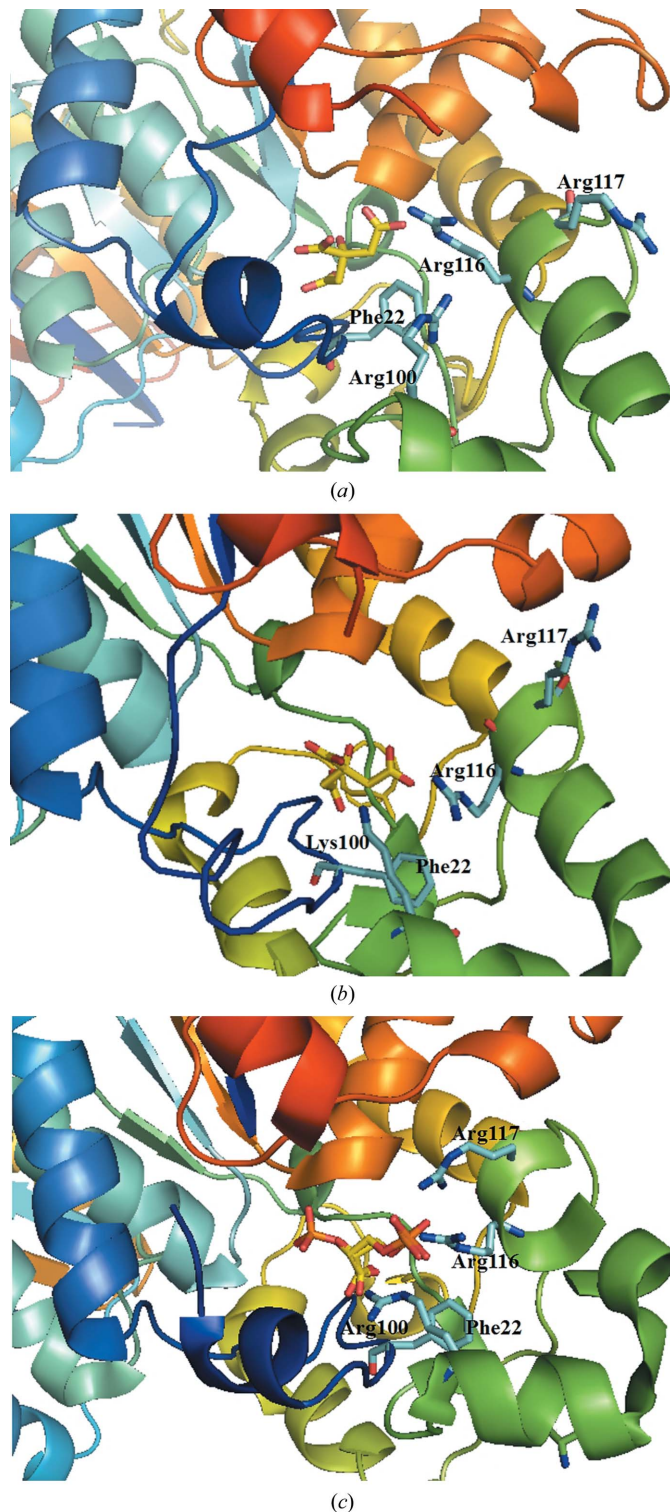
present, with the 3-phosphate group, rather than the 2-phosphate group, interacting with Arg116 NH2. A separate occupancy refinement of the side chain of Arg117 has also been measured as 69% directed outwards from the binding pocket. Fig. 3 shows the alternative conformations of these two Arg residues.

Isothermal titration calorimetry was used to characterize the interaction between BPGAM and the inhibitor citrate. The binding of citrate to BPGAM produced small endothermic enthalpy changes (Fig. 4). Following correction for the heat effects of dilution, the titration data were found to be consistent with an average apparent association constant K_a of 12 515 M^{-1} (corresponding to a K_d of 80 μM). Mutase inhibition assays gave a K_i value of 4.85 mM for citrate. This K_i value is much larger than the K_d value determined by ITC; however, the apparent K_i value may be a reflection of the complexity of the reaction mechanism (Nairn et al., 2000) rather than the citrate–BPGAM affinity.

4. Discussion

We have determined the crystal structure of human BPGAM in the absence of any ligand to 1.94 Å resolution. A number of differences between this structure and previously published lower resolution structures were noted. In our structure all residue side chains are present with the exception of the initiating methionine. Disordered areas of electron density beyond residue 250 are most likely to reflect the well documented flexibility of residues 250–263 of the protein. When compared with the structure of the BPGAM–BPG complex
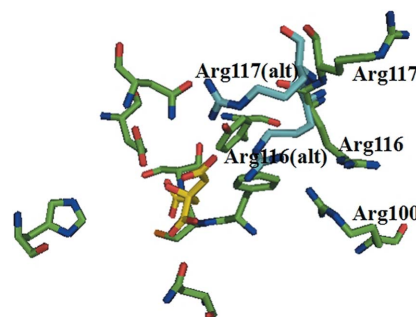

(a)

(b)

(c)

Figure 2
Comparison of citrate and BPG binding sites of BPGAM and PGAM. (a) Citrate (yellow) modelled into the binding pocket of BPGAM (PDB entry 3nfy). (b) Citrate–PGAM interactions (PDB entry 1yfk), with citrate shown in yellow. (c) BPG–BPGAM interactions (PDB entry 2hhj), with BPG shown in yellow.

Figure 3
Citrate (yellow) modelled into the binding pocket of BPGAM (PDB entry 3nfy), with alternative liganded Arg116/Arg117 side-chain conformations (from PDB entry 2hhj) shown in blue.
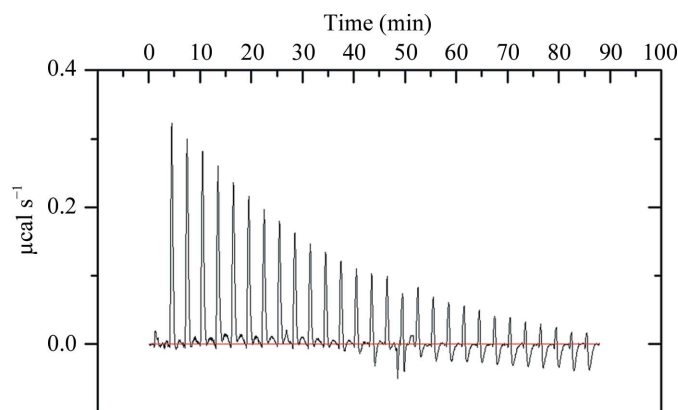

Figure 4
ITC analysis of citrate binding to BPGAM. Typical ITC data are shown for the binding of citrate to BPGAM at 298 K in 30 mM Tris–HCl pH 8.0. Analysis of this titration gave a K_d value for the BPGAM–citrate complex of 80 μM.
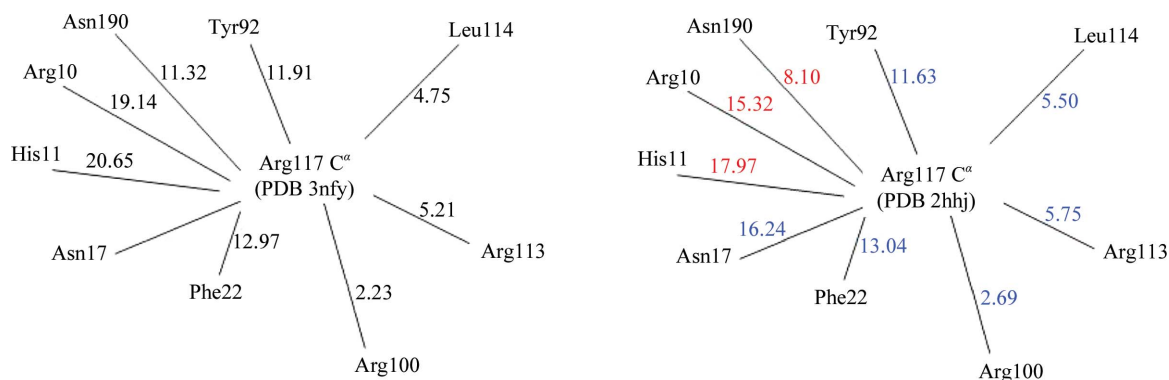
Figure 5
Distances between the C$^\alpha$ atom of Arg117 and the C$^\alpha$ atoms of other residues in the binding pockets of BPGAM (3nfy) and the BPGAM–BPG complex (2hhj). All distances are given in Å; those in red indicate the distances that are reduced in the BPGAM–BPG complex.

(PDB code 2hhj; Wang *et al.*, 2006), it is clear that movement of the binding-site residues Arg116 and Arg117 has occurred on binding of the substrate. These two flexible side chains can be seen to assume a conformation in which they are effectively 'trapping' the 2,3-BPG at the binding site, forming hydrogen-bonded contacts. In particular, Arg117 shows a very large movement, with the NH atoms having moved by more than 13 Å. An overlay of the BPGAM–BPG structure (2hhj) shows a movement of the C$^\alpha$ atom of Arg117 of 3.35 Å towards the opposite side of the binding pocket (occupied by Arg10, His11 and Asn190). While the distances between Arg117 C$^\alpha$ and His11 C$^\alpha$, Arg10 C$^\alpha$ and Asn190 C$^\alpha$ have decreased by 2.68, 3.82 and 3.22 Å, respectively, the distances between Arg117 and other residues important in ligand binding remain comparable (Fig. 5). Movement of the Arg at position 100 is also apparent. The distance between Arg100 C$^\alpha$ and Phe22 CZ is 5.1 Å in the BPGAM–BPG structure, whereas in the unliganded structure this distance is 8.29 Å. These large side-chain and backbone movements and the associated ligand–residue interactions effectively close off the binding site.

Inspection of the BPGAM–BPG structure (Wang *et al.*, 2006) suggests that citrate could interact with BPGAM, making similar contacts to those made by BPG. While a number of structural features of 2,3-BPG are distinct from those of citrate, the numbers and locations of hydrogen-bond donors and acceptors are comparable. We modelled citrate into our BPGAM structure (3nfy) with direct hydrogen-bond contacts between Tyr92 OH and citrate O1, between Asn17 OD1 and citrate O6 and O5, between Cys23 N and citrate O4 and between Glu89 OE2 and citrate O3 and O7. This compares well with the PGAM–citrate structure (1yfk), in which direct hydrogen bonds are formed between Ser23 N and Ser23 OG and citrate O4, between Asn17 OD1 and citrate O5 and between Lys100 NZ and citrate O6. As Lys100 is substituted by an arginine in BPGAM, it seems likely that backbone and side-chain movements bring this Arg into hydrogen-bonding distance of citrate O6 on binding BPGAM. Indeed, direct hydrogen-bond contacts can be seen between Arg100 and BPG in the BPGAM–BPG structure (2hhj), in which Arg117, Arg116, Cys23, Glu89, Asn17, Arg62, Arg10 and Gly189 also contribute to direct hydrogen-bonded contacts.

Citrate is a known inhibitor of many central metabolic enzymes, including 6-phosphofructokinase (K_d = 20 µM; Newsholme *et al.*, 1977; Ogawa & Atkinson, 1985; Colombo *et al.*, 1975) and isocitrate dehydrogenase (K_i = 160 µM; Popova *et al.*, 2007). It is also an effective inhibitor of members of the acid phosphatase superfamily, including 6-phosphofructo-2-kinase (K_i = 35 µM for kinase activity; Ventura *et al.*, 1992). Our ITC measurements suggest that citrate binds BPGAM with a K_d value of 80 µM. The significance of this value is supported by the K_m value of 300 µM for BPG (mutase

activity of BPGAM; Ravel *et al.*, 1997). Given that citrate and BPG share similar size and charge properties, they are likely to form similar multiple electrostatic interactions with the basic residues located at the entrance to the BPGAM active site.

5. Conclusions

We have presented the X-ray crystal structure of human bisphosphoglycerate mutase crystallized in the absence of any ligand and thus are able to give details of the dynamic nature of the ligand-binding residues for the first time. Modelling of the structure into electron density and comparison with known structures has identified substantial movements of side chains at the binding pocket in the presence and absence of ligand.

The modelling of citrate into the binding pocket which we have described in this paper was guided by the published structures of PGAM–citrate and BPGAM–BPG (Wang *et al.*, 2005, 2006) and we are confident that our model will be very similar to any future BPGAM–citrate complex which is solved. We anticipate that our BPGAM–citrate model will be a useful tool for the design of potential inhibitors of BPGAM phosphatase activity, although it is clear that any useful inhibitor will have to incorporate nonpolar features (*e.g.* heterocycles or hetero-substituted phenyl groups) to allow it to cross lipid bilayers since citrate itself is predominantly a trianion at pH 7.

It should be noted that ~30% of molecules in the crystal lattice have the side chains of Arg116 and Arg117 close to the expected conformation in the presence of ligand. This indicates a high degree of flexibility, which will require consideration when designing potential ligands for the active site of BPGAM.

References

Arnone, A. (1972). *Nature (London)*, **237**, 146–149.
Arslan, E., Sierko, E., Waters, J. H. & Siemionow, M. (2005). *Am. J. Surg.* **190**, 456–462.
Benesch, R. & Benesch, R. E. (1969). *Nature (London)*, **237**, 146–149.

structural communications

Berger, H., Jänig, G. R., Gerber, G., Ruckpaul, K. & Rapoport, S. M. (1973). *Eur. J. Biochem.* **38**, 553–562.

Bond, C. S., White, M. F. & Hunter, W. N. (2001). *J. Biol. Chem.* **276**, 3247–3253.

Bond, C. S., White, M. F. & Hunter, W. N. (2002). *J. Mol. Biol.* **316**, 1071–1081.

Collaborative Computational Project, Number 4 (1994). *Acta Cryst.* D**50**, 760–763.

Colombo, G., Tate, P. W., Girotti, A. W. & Kemp, R. G. (1975). *J. Biol. Chem.* **250**, 9404–9412.

Crowhurst, G. S., Dalby, A. R., Isupov, M. N., Campbell, J. W. & Littlechild, J. A. (1999). *Acta Cryst.* D**55**, 1822–1826.

Emsley, P. & Cowtan, K. (2004). *Acta Cryst.* D**60**, 2126–2132.

Fothergill-Gilmore, L. A. & Watson, H. C. (1989). *Adv. Enzymol. Relat. Areas Mol. Biol.* **62**, 227–313.

Higgins, M. J. & Klein, H. G. (1989). *J. Int. Care Med.* **4**, 221–233.

Ho, J., Sibbald, W. J. & Chin-Yee, I. H. (2003). *Crit. Care Med.* **31**, 687–697.

Högman, C. F. (1998). *Vox Sang.* **74**, 177–187.

Högman, C. F., Knutson, F., Lööf, H. & Payrat, J. M. (2002). *Transfusion*, **42**, 824–829.

Jedrzejas, M. J., Chander, M., Setlow, P. & Krishnasamy, G. (2000). *J. Biol. Chem.* **275**, 23146–23153.

Kuntz, I. D., Blaney, J. M., Oatley, S. J., Langridge, R. & Ferrin, T. E. (1982). *J. Mol. Biol.* **161**, 269–288.

McNae, I. W., Kan, D., Kontopidis, G., Patterson, A., Taylor, P., Worrall, L. & Walkinshaw, M. D. (2005). *Crystallogr. Rev.* **11**, 61–71.

Mulquiney, P. J., Bubb, W. A. & Kuchel, P. W. (1999). *Biochem. J.* **342**, 556–580.

Mulquiney, P. J. & Kuchel, P. W. (1999*a*). *Biochem. J.* **342**, 581–596.

Mulquiney, P. J. & Kuchel, P. W. (1999*b*). *Biochem. J.* **342**, 597–604.

Nairn, J., Duncan, D., Price, N. E., Kelly, S. M., Fothergill-Gilmore, L. A., Uhrinova, S., Barlow, P. N., Rigden, D. & Price, N. C. (2000). *Eur. J. Biochem.* **267**, 1–11.

Nairn, J., Krell, T., Coggins, J. R., Pitt, A. R., Fothergill-Gilmore, L. A., Walter, R. & Price, N. C. (1995). *FEBS Lett.* **359**, 192–194.

Newsholme, E. A., Sugden, P. H. & Williams, T. (1977). *Biochem. J.* **166**, 123–129.

Nukui, M., Mello, L. V., Littlejohn, J. E., Setlow, B., Setlow, P., Kim, K., Leighton, T. & Jedrzejas, M. J. (2007). *Biophys. J.* **92**, 977–988.

Ogawa, Y. & Atkinson, D. E. (1985). *Biochemistry*, **12**, 954–958.

Popova, T., Carvalho, M. A., Matasova, L. & Medvedeva, L. (2007). *Mol. Cell. Biochem.* **294**, 97–105.

Raat, N. J., Verhoeven, A. J., Mik, E. G., Gouwerok, C. W., Verhaar, R., Goedhart, P. T., de Korte, D. & Ince, C. (2005). *Crit. Care Med.* **33**, 39–45.

Ravel, P., Craescu, C. T., Arous, N., Rosa, J. & Garel, M. C. (1997). *J. Biol. Chem.* **272**, 14045–14050.

Rigden, D. J., Lamani, E., Mello, L. V., Littlejohn, J. E. & Jedrzejas, M. J. (2003). *J. Mol. Biol.* **328**, 909–920.

Rigden, D. J., Walter, R. A., Phillips, S. E. V. & Fothergill-Gilmore, L. A. (1999*a*). *J. Mol. Biol.* **286**, 1507–1517.

Rigden, D. J., Walter, R. A., Phillips, S. E. V. & Fothergill-Gilmore, L. A. (1999*b*). *J. Mol. Biol.* **289**, 691–699.

Rose, Z. B. (1982). *Methods Enzymol.* **87**, 42–51.

Sheldrick, G. M. (2008). *Acta Cryst.* A**64**, 112–122.

Tinmouth, A. & Chin-Yee, I. (2001). *Transfus. Med. Rev.* **15**, 91–107.

Uhrinova, S., Uhrin, D., Nairn, J., Price, N. C., Fothergill-Gilmore, L. A. & Barlow, P. N. (2001). *J. Mol. Biol.* **306**, 275–290.

Ventura, F., Rosa, J. L., Ambrosio, S., Pilkis, S. J. & Bartrons, R. (1992). *J. Biol. Chem.* **267**, 17939–17943.

Wang, Y., Liu, L., Wei, Z., Cheng, Z., Lin, Y. & Gong, W. (2006). *J. Biol. Chem.* **281**, 39642–39648.

Wang, Y., Wei, Z., Bian, Q., Cheng, Z., Wan, M., Liu, L. & Gong, W. (2004). *J. Biol. Chem.* **279**, 39132–39138.

Wang, Y., Wei, Z., Liu, L., Cheng, Z., Lin, Y., Ji, F. & Gong, W. (2005). *Biochem. Biophys. Res. Commun.* **331**, 1207–1215.

Wu, S., Dornan, J., Kontopidis, G., Taylor, P. & Walkinshaw, M. D. (2001). *Angew. Chem. Int. Ed.* **40**, 582–586.